Journal of Achievements in Materials and Manufacturing Engineering
International Scientific Journal published monthly by the World Academy of Materials and Manufacturing Engineering

Parametric optimization of dissimilar delding of AISI 409 ferritic stainless steel to AISI 316L austenitic stainless steel by using PCA method

N. Ghosh *, P. Kumar Pal, G. Nandi
Mechanical Engineering Department, Jadavpur University, Kolkata 700032, W.B, India
* Corresponding e-mail address: nabendu2003_ghosh@yahoo.co.in

ABSTRACT

Purpose: Taguchi design has been adopted in order to identify optimal parametric combination for desired quality of weld. Microscopy was conducted to study the effect of welding input process parameters (welding current, gas flow rate and nozzle to plate distance) on MIG weld microstructures of AISI 409 ferritic stainless steel and AISI 316L austenitic stainless steel.

Design/methodology/approach: A plan of experiments based on Taguchi technique has been used.

Findings: The present work is planned to investigate some perspectives of GMAW dissimilar joints between AISI 409, a ferritic stainless steel and AISI 316L a austenitic stainless steel.

Research limitations/implications: The main objective of the present study was to apply the Taguchi method to establish the optimal set of control parameters for the welding. The Taguchi method is employed to determine the optimal combination of design parameters, including: current, gas flow rate and nozzle to plate distance. the observed data have been interpreted, discussed and analyzed by considering yield strength , ultimate tensile strength and percentage of elongation combined with use of principal component analyses (pca) method.

Practical implications: Dissimilar welding is the joining between two different materials by any welding process. Dissimilar weld has made considerable attention in many fields, such as in ship industries and nuclear power plant.

Originality/value: The result computed is in form of contribution from each parameter, through which optimal parameters are identified for maximum tensile strength and percentage elongation. This paper presents new results of optimization using principal component analyses.

Keywords: Optimization; Dissimilar mig welding; AISI316l austenitic stainless steel; AISI 409 ferritic stainless steel; X-ray radiographic test; Tensile test

Reference to this paper should be given in the following way:

N. Ghosh, P. Kumar Pal, G. Nandi, Parametric optimization of dissimilar welding of AISI 409 ferritic stainless steel to AISI 316L austenitic stainless steel by using PCA method, Journal of Achievements in Materials and Manufacturing Engineering 75/1 (2016) 24-33.

MANUFACTURING AND PROCESSING

1. Introduction

Dissimilar metal joints are used in various engineering applications such as nuclear power plant, coal fired boilers, automobile manufacturing industry etc. Very often joining of dissimilar metals utilizes pressure welding instead of other joining methods [1]. However, GMAW is a versatile process to weld a wide range of dissimilar materials with high quality and productivity. Gas metal arc welding is one of the several arc welding processes, in which welding is done with an externally supplied gas shield which tries to protect the arc and molten puddle; the arc is formed between a consumable metal electrode and the work piece. GMAW process is commonly chosen for welding large metal structures such as bridges, automobiles, aircraft, aerospace craft and ships owing to its ability to produce good quality of weld with desired deposition rate.

Joining dissimilar materials is often more difficult than joining the same material or alloys with minor differences in composition. However, many dissimilar materials can be joined successfully with the appropriate joining process and specialized procedures. Sometimes situations frequently arise in which it becomes necessary to weld an austenitic stainless steel to mild or low alloy ferritic steel in nuclear power plant, ship industries, automobile industries etc. In selecting a suitable electrode, the effect of dilution of the weld metal by the base material must be considered. Dissimilar weld must possess sufficient tensile strength and ductility, so that the joint will not fail within the weld or HAZ. In the present work, dissimilar joints between AISI 409 ferritic stainless steel and AISI 316L austenitic stainless steel, are made by GMAW using ESAB AUTO rod 316L as filler wire.

Ferritic stainless steels with 11-12% chromium have been widely used as low cost utility stainless steels and have been developed to fill the gap between stainless steels and the rust-prone carbon steels, thus providing an alternative that displays both the advantages of stainless steels and engineering properties of carbon steels [2]. Typical applications for ferritic stainless steels include petrochemical, automotive exhaust systems, heat exchangers etc. Type 316L is austenitic chromium- nickel stainless steel containing molybdenum. Type 316L is an extra-low carbon version of Type 316 that minimizes harmful carbide precipitation due to welding. Ferritic and austenitic dissimilar welded joints are more or less used in petrochemical, ship industries and nuclear power plant [2].

Taban. E et al. [2] investigated the effects of dissimilar welds between ferritic stainless steel modified 12%Cr and carbon steel. Jeong Kil Kim et al [3] studied microstructure and high temperature properties of the dis similar weld between ferritic stainless steel STS441and SS400 carbon steel. H. Tasalloti, [4] et al. studied the effects of welding wire and torch weaving on GMAW of S355MC and AISI 304L dissimilar welds. Rosado et al. [5] utilized the eddy currents probe to detect the imperfections in friction stir welds of aluminium. Hu et al. [11] also employed a high-precision magnetic sensor to detect the weld defects in aluminium friction stir welds. Yilmaz and Uzun [12] compared the results obtained from destructive tests for mechanical properties of austenitic stainless steel (AISI 304L and AISI 316L plates, of 5 mm thickness) joints welded by GMAW and GTAW processes. The joints were made by GMAW process using ER 316 L Si filler metal and by GTAW process using ER 308L and ER 316L filler metals.

Dissimilar metal welding involves the joining of two or more different metals or alloys. In dissimilar metal welding, base metal contributes 15% dilution from each metal while the filler metal contributes 70% to the total weld nugget composition. When welding dissimilar metals, good solid solubility is essential for sound weld properties. The trends of welding dissimilar metals present considerable challenges. Welding of dissimilar metals has attracted attention of the researchers worldwide, owing to its many advantages and challenges. There is no denial in the fact that dissimilar welded joints offer more flexibility in the design and production of the commercial and industrial components. Dissimilar Welding of ferritic and austenitic stainless steel in general and GMAW welding of such steel in particular, can well be considered as one of the areas where more extensive research may contribute, in a significant way, to the precise control of the welding process for better and acceptable quality of weldment.

Weld quality mainly depends on features of bead geometry, mechanical-metallurgical characteristics of the weld as well as on various aspects of weld chemistry and these features are expected to be greatly influenced by various input parameters like current, voltage, electrode stick-out, gas flow rate, edge preparation, position of welding, welding speed and many more. Moreover, the cumulative effect of the mentioned quality indices determines the joint strength that should meet the functional aspects of the weld in the practical field of application. Therefore, preparation of a satisfactory good quality weld seems to be a challenging job. The survey of literature has shown that, various statistical techniques such as regression analysis, response surface methodology (RSM) and Taguchi method have been adopted by many researchers to modelling and optimization of weld bead geometry in GMAW [6-10].

Taking these into consideration, the present work is planned to investigate some perspectives of GMAW

dissimilar joints between AISI 409, a ferritic stainless steel and AISI 316L a austenitic stainless steel.

2. Experimental plan, set-up and procedure

In the present work, experiments are done in a planned experimental order Taguchi Orthogonal array design L9 has been used as design of experiment. As mentioned earlier, welding current, gas flow rate and nozzle to plate distance are selected as input parameters and three levels are considered for each of them. Welding process parameters and their levels are shown in Table 1. Welding Design Matrix as per L9 Taguchi Orthogonal Array Design is shown in Table 2. The Photographic view of welding set up and one welded sample are shown in Figure 1.

Table1.
Welding process parameters and their levels

Factors	Unit	Notation	Levels		
			1	2	3
Welding Current	A	C	100	112	124
Gas Flow rate	l/min	F	10	15	20
Nozzle to Plate Distance	mm	S	9	12	15

Table 2.
Welding Design Matrix as per L9 Taguchi Orthogonal Array Design of matrix

Welding Current (A)	Gas flow rate (*l*/min)	Nozzle to plate distance (mm)
1	1	1
1	2	2
1	3	3
2	1	2
2	2	3
2	3	1
3	1	3
3	2	1
3	3	2

Dissimilar weld joints between austenitic stainless steel AISI 316L and ferritic stainless steel AISI 409 each of dimension 100 mm x 65mm x 3 mm are joined by MIG welding process by using austenitic filler wire AISI 316 L. No edge preparation is used as it is not recommended for welding of 3 mm thick austenitic stainless steel. Diameter of the electrode wire is selected 1.2 mm.

Fig. 1. Photographic view of welding set-u

Welding has been done on ESAB make AUTO K-400 MIG/MAG welding machine. Butt welded joints being done under varied input parameters, visual inspection and X-ray radiographic test of all welded specimens has been made. After visual inspections and X-ray radiographic test, tensile test specimens have been prepared from the welded joints, by cutting/machining.

During cutting/machining of the tensile test specimens, small size cut pieces also been made. This small size-cut pieces have then been ground, polished and etched for studying microstructures. Results of Visual inspection and X-ray radiographic tests are reported in section 3. Analysis of microstructure will be considered as a separate and detailed work with minute details. The tensile test specimens have been tested on tensile testing machine INSTRON as per ASTM standard. The major specifications of the tensile testing machine INSTRON are given below.

- Model No.: 5589,
- Serial No.: 95/1058,
- Maximum capacity: 600 KN.

A schematic diagram showing the basic dimensions of the tensile test specimens of thickness 3 mm is given in Figure 2.

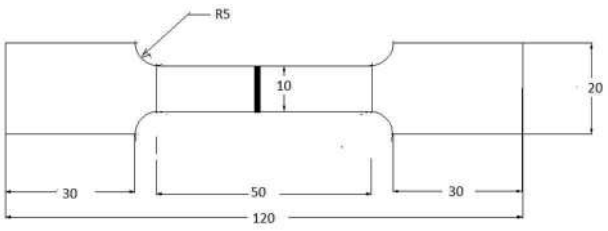

Fig. 3. Schematic diagram of the specimen prepared for tensile test

3. Results of visual inspection and X-ray radiographic test and discussion

For visual inspection, the weld surfaces are observed with the naked eye, in order to detect the surface defects of the weldment. X-ray radiographic tests have been conducted for all the 9 samples by XXQ-2005 X-ray flaw detector. Results of Visual Inspection and X-ray radiographic test is shown in Table 3.

Table 3.
Result of visual inspection and X-ray radiographic test

Sample no.	Result of visual inspection	Result of X-ray radiographic tests
1	no defects	no defects
2	blow hole, spatter	porosity
3	excessive deposition, spatter	lack of fusion
4	no defects	no defects
5	spatter, uneven penetration	porosity
6	no defects	no defects
7	uneven penetration undercut	porosity
8	uneven penetration	lack of fusion
9	no defect	no defect

It is observed from the results of visual inspection and X-ray radiographic test that, sample nos.1, 4, and 6 are almost defect free. Some minor defects like weld depression, a little bit porosity etc. has been found in sample nos. 2, 3, 5, 7, 8 and 9. However, defects like lack of penetration, undercut at both root and face, lack of side wall fusion, blow hole, porosity etc. are observed in some of the other samples. The copies of X-ray radiographic films are presented in Figures 4-9.

Fig. 4. Copies of X-ray radiographic film for sample no. 4

Fig. 5. Copies of X-ray radiographic film for sample no. 8

Fig. 6. Copies of X-ray radiographic film for sample no. 3

Fig. 7. Copies of X-ray radiographic film for sample no. 5

Fig. 8. Copies of X-ray radiographic film for sample no. 7

Fig. 9. Copies of X-ray radiographic film for sample no. 2

If the results of visual inspection and X-ray radiographic tests are compared, some consistency in the findings can be noticed. The individual and combined effects of the levels of gas flow rate, current and nozzle to plate distance have been reflected in the samples as defects like lack of penetration, undercut, lack of fusion, uneven deposition and weld depression. Further, the skill of the welder is a significant factor influencing weld quality. Defects may come from any irregularities in the base metal and filler wire also. Any improper welding arrangements can also lead to the significant defects. Improper selection of welding parameters like welding current, gas flow rate and nozzle to plate distance can also create welding defects. Radiographic films for Samples Nos. 1, 4, 6 and 9 are almost defect-free. These samples are welded with low current and low nozzle to plate distance.

Undercut is possibly caused by improper joint geometry for some of the samples. It may have been resulted due to excessive current, voltage, large nozzle to plate distance as well. The combined effects of welding parameters can also create undercut. Table 3 indicates that undercuts have been found in sample no.7. Undercut normally occurs due to use of high current, high nozzle to plate distance and low gas flow rate.

Lack of fusion at root or wall has occurred possibly due to improper setting of the current, improper cleaning, faster arc travel speed, presence of oxides, scale and other impurities which do not permit the deposited metal to fuse properly with the base metal. Too low heat input does not ensure proper melting of the weld deposit. With too high heat input, the weld pool becomes too large and starts to flow away in the area in front of the arc which prevents melting of the base metal. Sample nos.3 may have suffered from lack of fusion due to lower heat input and high nozzle to plate distance. Lack of penetration is a major problem affecting the strength of the weld. This may come from lower heat input; faster travel speed, improper selection of currents etc.

Porosity has been found in sample nos. 2, 5, and 7 which may have resulted from gas being entrapped in the solidifying metal. Blow holes have been observed in sample no. 2, larger arc, faster travel rate, damp filler rod, unclean job surface etc. may be the possible reasons. Faster gas flow rate is a cause of porosity. All the samples showing porosity is found to be welded with high gas flow rate and large nozzle to plate distance.

4. Study of microstructures and discussion

Study of microstructures has been made for the welded samples and the photographs are taken of base metal, HAZ and weld region by the Leica DM LM metallurgical microscope. The representative microstructures are given in Figures10-15.

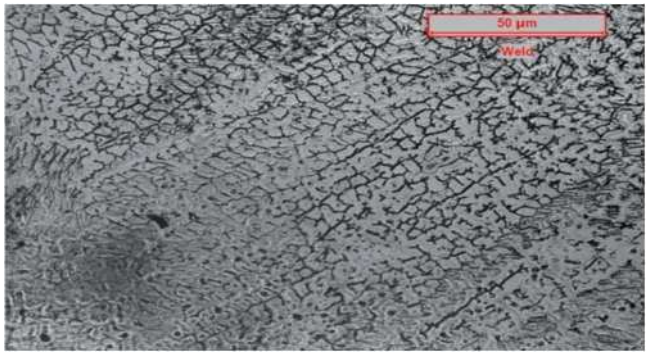

Fig. 10. Metallographic view of sample number 3: WELD

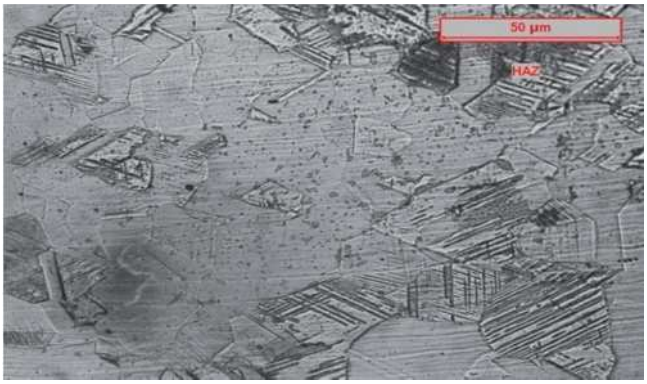

Fig. 11. Metallographic view of sample number 3. HAZ

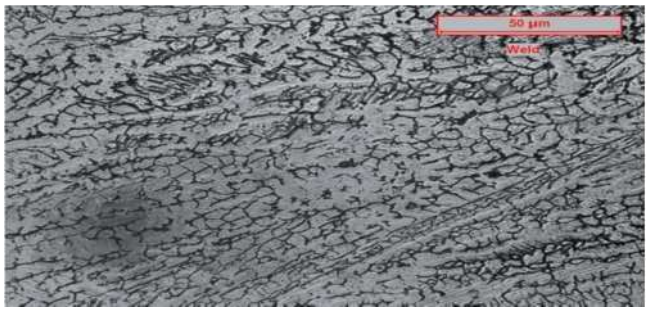

Fig. 12. Metallographic view of sample number 4. WELD

In so far as the micro-structure of base metal is concerned, pure austenitic grains with twin boundaries are observed in all the samples. One representative base metal microstructure is shown in Figure16. Not much variation is observed among the HAZ microstructures of 9 samples.

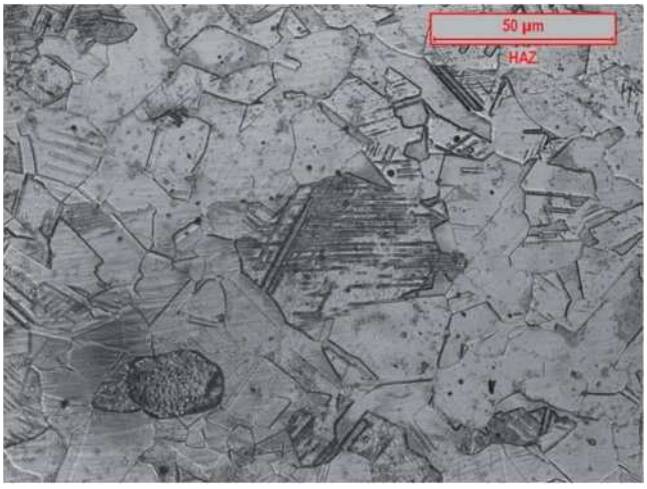

Fig. 13. Metallographic view of sample number 4. HAZ

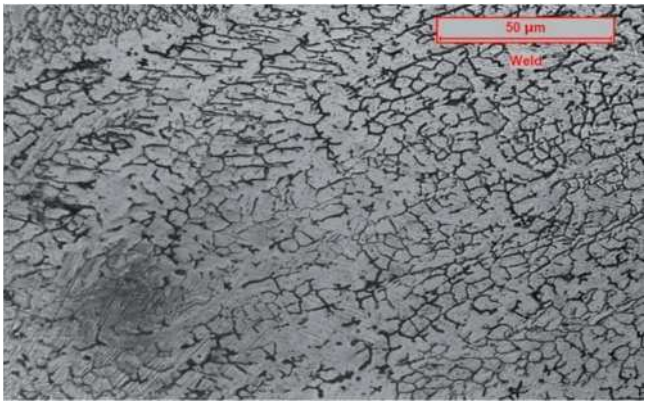

Fig. 14. Metallographic view of sample number 6. WELD

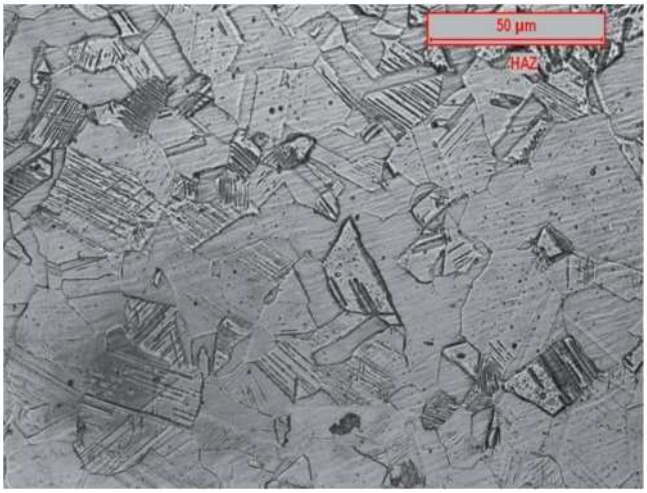

Fig. 15. Metallographic view of sample number 6. HAZ

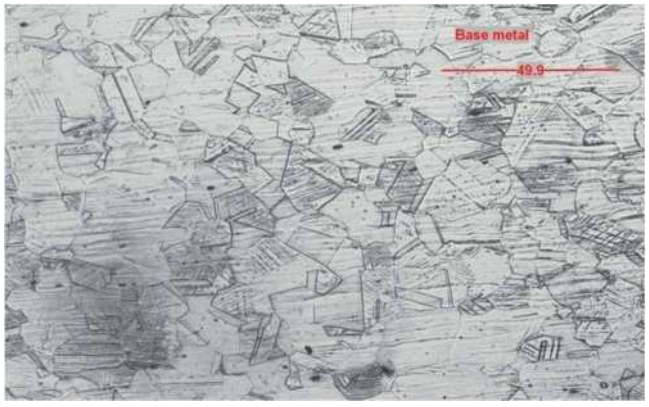

Fig. 16. Metallographic view of sample number 6. BASE

In general, HAZ microstructures are not found to be much different from base metal microstructure. However, grains are found to be coarser in HAZ than in base metal. This may be attributed to lower cooling rate in the HAZ region. Results of micro-hardness test are in consistent with the above observation (HAZ hardness is found lower than the hardness of the base metal). Austenitic twins are also observed in the HAZ of all the samples. In almost all the samples, traces of δ- ferrite are observed in HAZ under the microscope. Sample no. 3 and 4 (Figures 11 and 13, respectively) show highest and lowest hardness values respectively in the HAZ region.

But no significant cause behind this has been found from microstructural study of HAZ. If weld metal microstructures of all the samples are compared with either base metal or HAZ microstructures, it is found that weld metal microstructure is looking very much different from HAZ and base metal microstructures. In most of the samples columner-dendritic grain growths are observed in the weld microstructure. In the weld-HAZ transition region, in some samples more amount of δ-ferrite is precipitated, because, dilution-less weld metal can not reach the base metal.

So, base metal is Variation in parametric condition has influenced microstructures of different zones of weldment, not in a very simple manner. But effect of change in welding parameters is definitely there. This aspect may be taken into account in an extensive manner in future work.

5. Tensile test results and discussion

Welding has been done on ESAB make AUTO K -400 MIG/MAG welding machine. Butt welded joints being done under varied input parameters, visual inspection and X-ray radiographic test of all welded specimens has been made. After visual inspections and X-ray radiographic test, tensile test specimens have been prepared from the welded joints, by cutting/machining.

The tensile test specimens, prepared corresponding to L_9 Taguchi orthogonal array design of experiments, have been tested for tensile strengths and the results obtained are given in Table 4. Results shown in Table 4 indicate that for many of the welded samples test results are satisfactory. The best result is obtained in sample no.3 (yield strength= 335.9 MPa and ultimate tensile strength=468.7 MPa). The worst result in tensile testing has been obtained for the sample no. 8 for both the responses. For this sample yield strength is 233.4 MPa and ultimate tensile strength is 366.6 MPa.

Table 4.
Tensile tests result

S. No	Output responses	
	Yield strength	Ultimate Tensile Strength, MPa
1	283	412.3
2	247.4	369.9
3	335.9	468.7
4	257.7	385.3
5	257.4	389.6
6	294.1	429.1
7	286.5	414.1
8	233.4	366.6
9	304	430.6

6. Optimization by using principal component analyses

Experimental data (Table 3) has been normalized first. The objective is to maximize the experimental data. For this purpose Higher-the-Better (HB) criteria is used. Data has been normalized using the equations shown below.

(a) LB (lower-the-better)

$$X_i^*(k) = \frac{minX_i(k)}{X_i(k)} \quad (1)$$

(b) HB (higher-the-better)

$$X_i^*(k) = \frac{X_i(k)}{maxX_i(k)} \quad (2)$$

where:
i = 1,2, ….., m;
k = 1,2, ….., n.

After data normalization a check has to be made whether responses are correlated or not.

Results of PCA (Eigen value, Eigen vector, accountability proportion AP and cumulative accountability proportion CAP) is shown in Table 5.

Table 5.
Eigen value, Eigen vector, accountability proportion AP and cumulative accountability proportion CAP)

	ψ 1	ψ 2
Eigen Values	1.9930	0.0070
Eigen vector	0.707 0707	-0.707 0.707
AP	0.997	0.003
CAP	0.997	1.000

Finally, multi-response performance index (MPI) has been computed using the following equation MPI= ψ_{1*}0.997 + ψ_{2*}0.003MPI has been treated as single objective function for optimization in order to maximize it. The factorial combination that maximized MPI can be treated as optimal parametric combination/ most favourable process environment ensuring high surface quality. This has been performed using Taguchi method.

Principal Component and Calculated MPI are shown in Table 6.

S/N ratio has been calculated using Higher-the-Better (HB) criteria. Optimal setting has been evaluated from this plot (Fig. 17). Predicted optimal combination becomes: C1F3S1. Optimal result has been verified through confirmatory test. According to Taguchi' prediction, predicted value of S/N ratio for MPI becomes 2.9856 whereas in confirmatory experiment it is obtained a value of 3.0920. So quality has improved using the optimal setting.

Table 6.
Principal component and calculated MPI

Sample No.	Yield strength, MPa	Ultimate tensile strength, MPa	Calculated MPI
1	1.21758	0.02627	1.21401
2	1.07869	0.03724	1.07557
3	1.414	0	1.40976
4	1.1236	0.03879	1.12035
5	1.12946	0.04591	1.12621
6	1.26629	0.02824	1.26257
7	1.22766	0.02162	1.22404
8	1.04425	0.06173	1.0413
9	1.28938	0.00967	1.28555

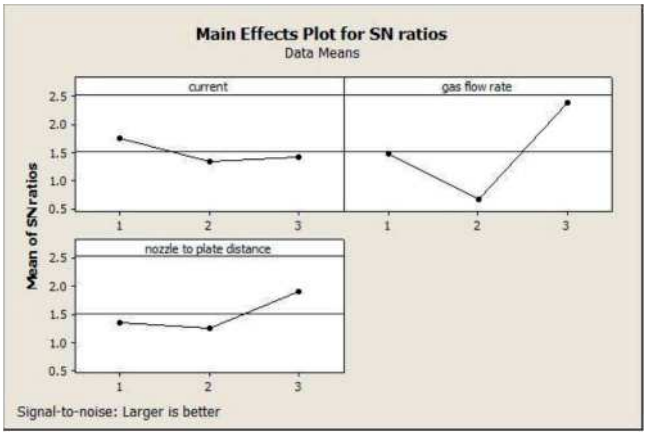

Fig. 17. Represents S/N ratio plot of MPI

7. Conclusions

For dissimilar joining of AISI 409 ferritic stainless steel to AISI 316L austenitic stainless steel, by GMAW, the

following conclusions are made based on the results of present investigation.

- Under certain combinations of parameters, GMAW of ferritic stainless steel to austenitic stainless steel provides satisfactory joints.
- Results of visual inspection indicate that undercut, blow holes and spatter occur in few samples; uneven deposition and excessive penetration have also been found in some samples.
- Results of X-ray radiography test indicate: lack of penetration, low-level porosity and lack of fusion in some of the samples.
- Results of visual inspection and X-ray radiographic tests when compared, some consistency in the results is found, mostly.
- Visual and X-ray radiographic tests also indicate that under some parametric conditions (corresponding to sample nos. 1, 4, 6 and 9), no significant defect occurs; the samples made under these conditions show good ultimate tensile strength.
- Pure austenitic structure with significant amount of austenitic twin is found in the microstructure of base metal. No significant difference is observed in the microstructure of HAZ with respect to base metal microstructure. However grain growth is observed in HAZ. Austenitic twins are also observed in HAZ. Small amount of δ-ferrite is observed in the microstructure of HAZ. Dispersed chromium carbides are found in some samples. Windmanstatten structure is found at some regions for few samples. Small amounts of δ-ferrite are also observed in certain portions of the weld zone. In some samples pure austenitic grains with almost no amount of δ-ferrites are found as well. Columner-dedritic grain growth is observed in almost all samples in the weld zone. But in some dispersed areas, equi-axed grain growth is observed. AF (Austenitic-ferritic) mode solidification is found to be predominant. But in some small areas FA mode (Ferritic-austenitic) of solidification is observed.
- With the help of mean main effect plots and S/N ratio plots, optimum parametric combination has been determined. The optimal factor setting becomes C1F3S3 (i.e. welding current=100 A, gas flow rate = 20 l/min and nozzle to plate distance =15 mm).

Acknowledgements

The authors sincerely thanks all the staff members of Blue Earth workshop of Jadavpur University who directly or indirectly made their involvement in the experimental work and testing part of this work. The authors are very much grateful to SKB Metallurgical Services, Salkia, Howrah for their cooperation and help.

References

[1] C. Rakesh, P. Riddhish, I. Asha, Reliability of dissimilar metal joints using fusion welding: a review, Proceedings of the International Conference on Machine Learning, Electrical and Mechanical Engineering, Dubai (UAE), 2014.

[2] E. Taban, E. Deleu, A. Dhooge, E. Kaluc, Evaluation of Dissimilar Welds between Ferritic Stainless Steel Modified 12% Cr and Carbon Steel S355, American Welding Society and the Welding Research Journal 8 (2012) 291-297.

[3] J.K. Kim, S.G. Hong, K.B. Kang, C.Y. Kang, Microstructure and high temperature properties of the dissimilar weld between ferritic stainless steel and carbon steel, Metals and Materials International 15/5 (2009) 843-849.

[4] H. Tasalloti, P. Kah, J. Martikainen, Effects of welding wire and torch weaving on GMAW of S355MC and AISI 304L dissimilar welds, International Journal of Advanced Manufacturing Technology 71 (2014) 197-205.

[5] L.S. Rosado, T.G. Santos, M. Piedade, P.M. Ramos, P. Vilaca, Advanced technique for non-destructive testing of friction stir welding of metals, Journal of Measurement 43 (2010) 1021-1030.

[6] P.S Rao, O.P. Gupta, S.N. Murty, A.B.K. Rao, Effect of process parameters and mathematical model for the prediction of bead geometry in pulsed GMA welding, International Journal of Advanced Manufacturing Technology 45/5-6 (2009) 496-505.

[7] R.S. Parmar, Welding Processes and Technology, Second Edition, Khanna Publications, New Delhi, 1997.

[8] O.P. Khanna, Welding Technology, Dhanpat Rai & Sons, 1986.

[9] A. Ghosh, A.K. Mallik, Manufacturing Science, East-West Press Private Limited, NewDelhi, 2008.

[10] R.L. Little, Welding and Welding Technology, McGraw Hill Book Company, New York, 1973.

[11] B, Hu, R. Yu, H. Zou, Magnetic non-destructive testing methods for thin-plates aluminium alloys, NDT&E International 47 (2012) 66-69.

[12] R. Yilmaz, H. Uzun, Mechanical properties of austenitic stainless steels welded by GMAW and GTAW, Journal of Marmara for Pure and Applied Sciences 18 (2002) 97-113.

[13] N. Murugan, R.S. Parmar, Effects of MIG process parameters on the geometry of the bead in the automatic surfacing of stainless steel, Journal of Materials Processing 41/4 (1994) 381-398.